Assembling Molecular Semiconductor Composite for Enhanced Photocatalytic Cyclohexene Oxidation

Haiyan Yu,[a] Xueting Wang,[a] Tingting Kong,[a] Mei-Yan Gao*[b] and Xiaofeng Cui*[a]

a. Anhui Engineering Research Center of Carbon Neutrality, The Key Laboratory of Functional Molecular Solids, Ministry of Education, College of Chemistry and Materials Science, Anhui Normal University, Wuhu 241002, Anhui, P. R. China.

b. Department of Chemical Sciences, Bernal Institute, University of Limerick, Limerick V94 T9PX, Republic of Ireland.

Experimental Procedures

Materials.

All reagents and solvents were used as received without further purification. Formic acid (HCOOH, ≥99%), Isopropanol (HO^iPr, ≥99%), were purchased from Sinopharm Chemical Reagent Co. Ltd. Isopropyl titanate ($Ti(O^iPr)_4$, ≥99.9%), Phosphotungstic acid (PTA, ≥99.9%) were purchased from Aladdin Reagent Inc.

Synthesis of Ti_{12}-oxo cluster.

$Ti(O^iPr)_4$ (3.68 mL, 12 mmol) and 0.4 mL of formic acid were mixed at room temperature. The resultant solution was sealed in a 25 mL vial and transferred to a preheated oven heated at 80 °C for about four days. After cooled to room temperature, colorless block crystals of Ti_{12}-oxo cluster were obtained.

Synthesis of Ti_{12}PTA.

Isopropanol (5.5 mL) and phosphotungstic acid (0.16 g, 0.054 mmol) were mixed at room temperature; then $Ti(O^iPr)_4$ (0.92 mL, 3.0 mmol) was added. The resultant solution was sealed in a 25 mL vial and transferred to a preheated oven heated at 80 °C for about three days. After cooled to room temperature, colorless block crystals of Ti_{12}PTA were obtained.

Sample characterizations.

Powder X-ray diffraction (PXRD) patterns were recorded with a diffractometer (SmartLab 9kw) using Cu Ka (k = 0.15406 nm) radiation with a Nickel filter operating at 40 kV and 10 mA at a scanning rate of $20°\cdot min^{-1}$. The scanning electron microscopy image of Ti_{12}PTA was taken on a Hitachi-Technologies Corporation Regulus8100 scanning electron microscopy operated at 15 kV. High-resolution TEM (HRTEM) images were taken on a Talos F200S-G2 field-emission high-resolution transmission electron microscope operated at 200 kV. Prior to electron microscopy characterizations, a drop of the isopropanol suspension of particles was placed on a piece of carbon-coated copper grid and dried under ambient conditions. The size of Ti_{12}PTA nanoclusters was measured from HRTEM images and the average particle diameter was calculated from the mean diameter frequency distribution with the formula: $d= \Sigma n_i d_i / \Sigma n_i$, where n_i is the number of particles with a particle diameter (d_i) in a certain range. High-resolution HAADF-STEM images were taken on a itan Cubed Themis G2300 Spherical aberration-corrected transmission electron microscope. X-ray photoelectron spectra (XPS) were collected on an Thermo ESCALab 250 X-ray photoelectron spectrometer, using monochromatized Al–Kα X-ray as the excitation source. Fourier-transform infrared (FT−IR) spectroscopy was performed on a Bruker Invenio. In-situ diffuse reflectance infrared Fourier transform spectroscopy (DRIFTS) over Ti_{12}PTA was performed by using a Bruker INVENIO S FT-IR spectrophotometer, equipped with an MCT detector cooled by liquid nitrogen and a commercial reaction chamber from Harrick Scientific. The sample was irradiated by the Xenon lamp through a quartz window, and the IR spectra were collected in situ through the MCT detector. Each spectrum was recorded by averaging 128 scans at a 4 cm^{-1} spectral resolution.

Photocatalytic oxidation of Cyclohexene.

Standards with given concentrations of all possible reactant and products, namely cyclohexene, cyclohexene oxide, 2-cyclohexene-1-ol, 2-cyclohexene-1-one, 1,2-cyclohexanediol and adipic acid were prepared. 10 μL of 1,2-dichlorobenzene was added to the standard as the internal standard. Using the area ratio vs. the mol ratio of a compound and the standard, calibration curves of each compound were generated. Standards of 1-hexene and cis-cyclooctene epoxidations were prepared analogously.

For the measurement of photocatalytic cyclohexene oxidation, 2 mg catalysts were dispersed in 10 mL cyclohexene in a 50 mL quartz flask. Then the quartz flask was performed on multi-channel photochemical reaction system (Perfect Light, PCX-50C) with 10 W LED lamp as the light source.

The atmosphere of quartz flask was replaced with high-purity O_2 nine times to form an oxidation ambient. The reaction temperature was kept constant at 25℃ by circulating condensate water. The power density of light source was measured to be 200 mW·cm^{-2}. The oxidation products were evaluated on a GC-MS (TRACE 1300 and ISQ 7000, thermo-scientific).

Electrochemical measurements.

Photocurrent was recorded with a CHI 660E electrochemical workstation via a conventional three-electrode system in 0.5 M sodium sulfate electrolyte. Working electrode was prepared as follows: 5 mg photocatalysts were dispersed in a mixed solution of 980 μL ethanol and 20 μL nafion dispersion solutions to generate a homogeneous slurry. This slurry was transferred and coated on ITO glass plates (1 cm × 2 cm), and then dried at room temperature. The platinum foil and Ag/AgCl electrode were used as the counter electrode and the reference electrode, respectively, in a 0.5 M Na_2SO_4 aqueous solution. The initial potential was set to 0.5 V (*vs.* Ag/AgCl). To investigate the underlying contribution for the photocurrent, triethanolamine was used as an electron donor to construct an outer-sphere reaction system under the same test conditions.

The Mott-Schottky plots were measured over an alternating current (AC) frequency of 1000, 1500 and 3000 Hz. The electrode was immersed in the 0.5 M Na_2SO_4 aqueous solution. Working electrode was prepared as follows: 5 mg photocatalysts were dispersed in a mixed solution of 980 μL ethanol and 20 μL nafion dispersion solutions to generate a homogeneous slurry. This slurry was transferred and coated on ITO glass plates (1 cm × 2 cm), and then dried at room temperature. Ag/AgCl and Pt sheet electrodes were used as reference electrode and counter electrode, respectively.

Detection of reactive species.

The experiments for determining reactive species were conducted by adding different types of excess scavengers (10 mM) into the stock solution before light irradiation. $AgNO_3$ was employed for sacrificing electrons, β-carotene for singlet oxygen ($^1O_2$), benzoquinone for $\bullet O_2^-$, tert-butanol for •OH, sodium sulfide for holes. $^1O_2$ was further confirmed with ESR spectroscopy by using 2,2,6,6-tetramethyl-4-piperidone hydrochloride to in situ trap the spin-reactive species. 5 mg catalysts were dispersed in 2.5 mL acetonitrile solution, and 500 μL 4-oxo-TMP was added.

Single crystal X-ray diffraction

Single crystal X-ray diffraction data of Ti_{12}PTA was collected on a Bruker Quest diffractometer equipped with a IμS microfocus X-ray source Mo Kα, (λ = 0.71073 Å) and CMOS detector. APEX4 was used for collecting, indexing, integrating and scaling the data.[S1] Absorption corrections were performed by multi-scan method.[S2] Space groups were determined using XPREP[S3] as implemented in APEX4. All non-hydrogen atoms present in the frameworks were refined anisotropically. Hydrogen atoms were located at idealized positions from the molecular geometry and refined isotropically with thermal parameters based on the equivalent displacement parameters of their carriers. The SQUEEZE option of PLATON was used to eliminate the contribution of disordered guest molecules to the reflection intensities.[S4] Crystallographic data reported in this paper is summarized in Tables S1. These crystal structures have been deposited to the Cambridge Crystallographic Data Centre.

Table. S1 Crystallographic data and refinement parameters of Ti_{12}PTA.

	Ti_{12}TPA
CCDC Number	2377155
Empirical formula	$C_{99}H_{231}O_{104}PTi_{24}W_{12}$ 1.4[C_3H_8O] 2[H_2O] 1.6[H_2O]
Formula weight	6621.58
Temperature/K	293(2)
Crystal system	monoclinic
Space group	$P2_1/n$
a/Å	15.7675(4)
b/Å	29.1952(7)
c/Å	44.3515(14)
α/°	90
β/°	91.927(2)
γ/°	90
Volume/Å^3	20405.0(10)
Z	4
ρ_{calc}g/cm^3	2.155
μ/mm^{-1}	7.707
Radiation	Mo Kα (λ = 0.71073)
Reflections collected	68433
Independent reflections	21885
Goodness-of-fit on F^2	1.055
R_1[I>2σ(I)][a]	0.0939
wR_2[I>2σ(I)][b]	0.2739

[a] $R_1 = \Sigma||F_o| - |F_c||/\Sigma|F_o|$. [b] $wR_2 = \{\Sigma[w(F_o^2 - F_c^2)^2]/\Sigma[w(F_o^2)^2]\}^{1/2}$.

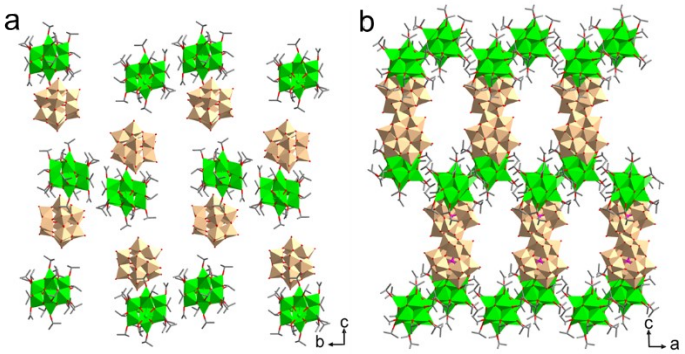

Fig. S1 Packing structure of Ti_{12}PTA viewed along a and b axis. H atoms are removed for clarity.

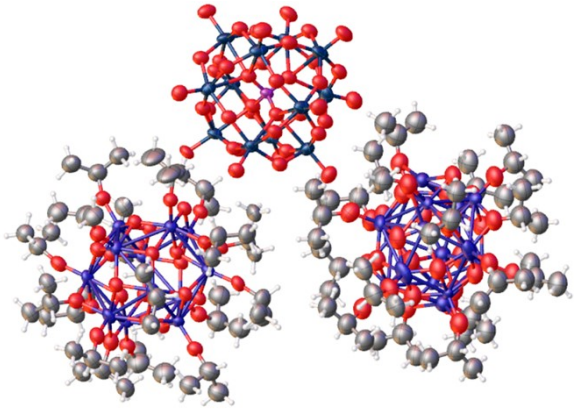

Fig. S2 ORTEP drawings of Ti_{12}PTA at the 50% probability level.

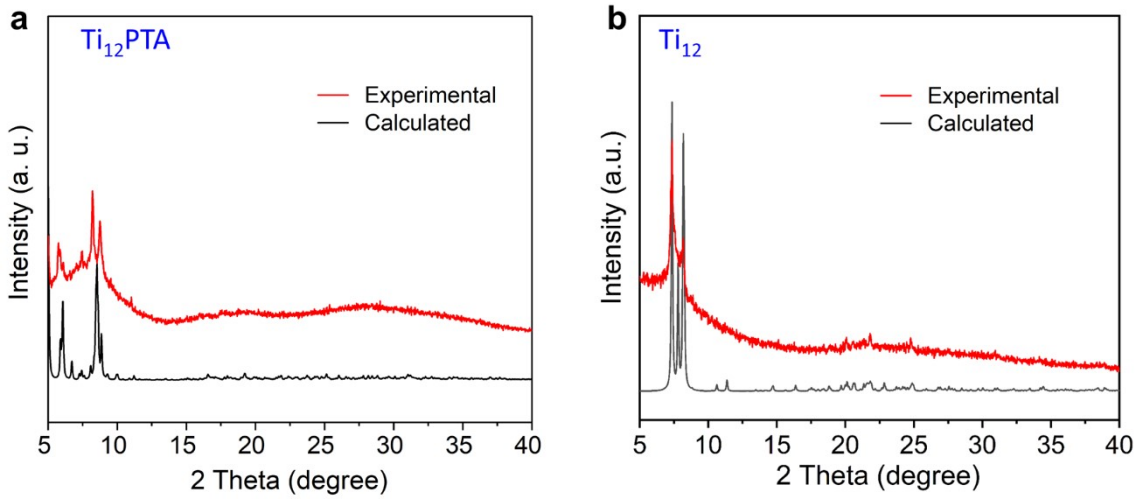

Fig. S3 PXRD patterns of (a) cocrystal Ti_{12}PTA and (b) pure Ti_{12}-oxo cluster.

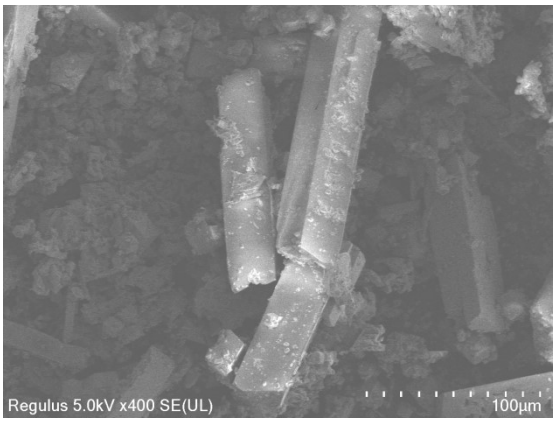

Fig. S4 The scanning electron microscopy image of Ti_{12}PTA.

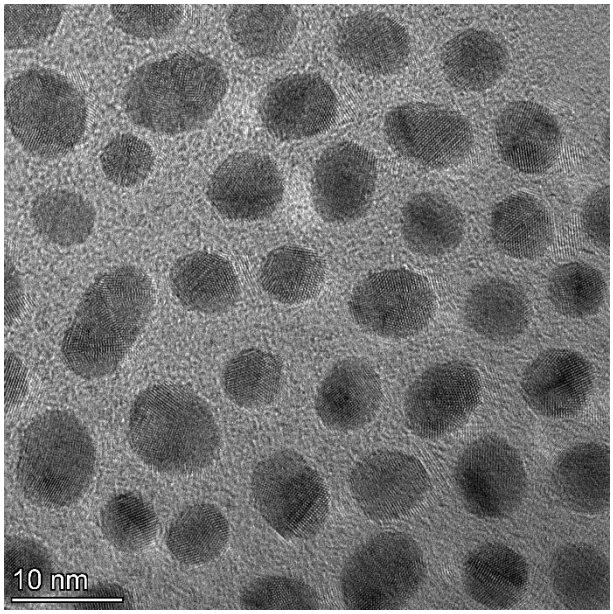

Fig. S5 The transmission electron microscopy image of Ti_{12}PTA.

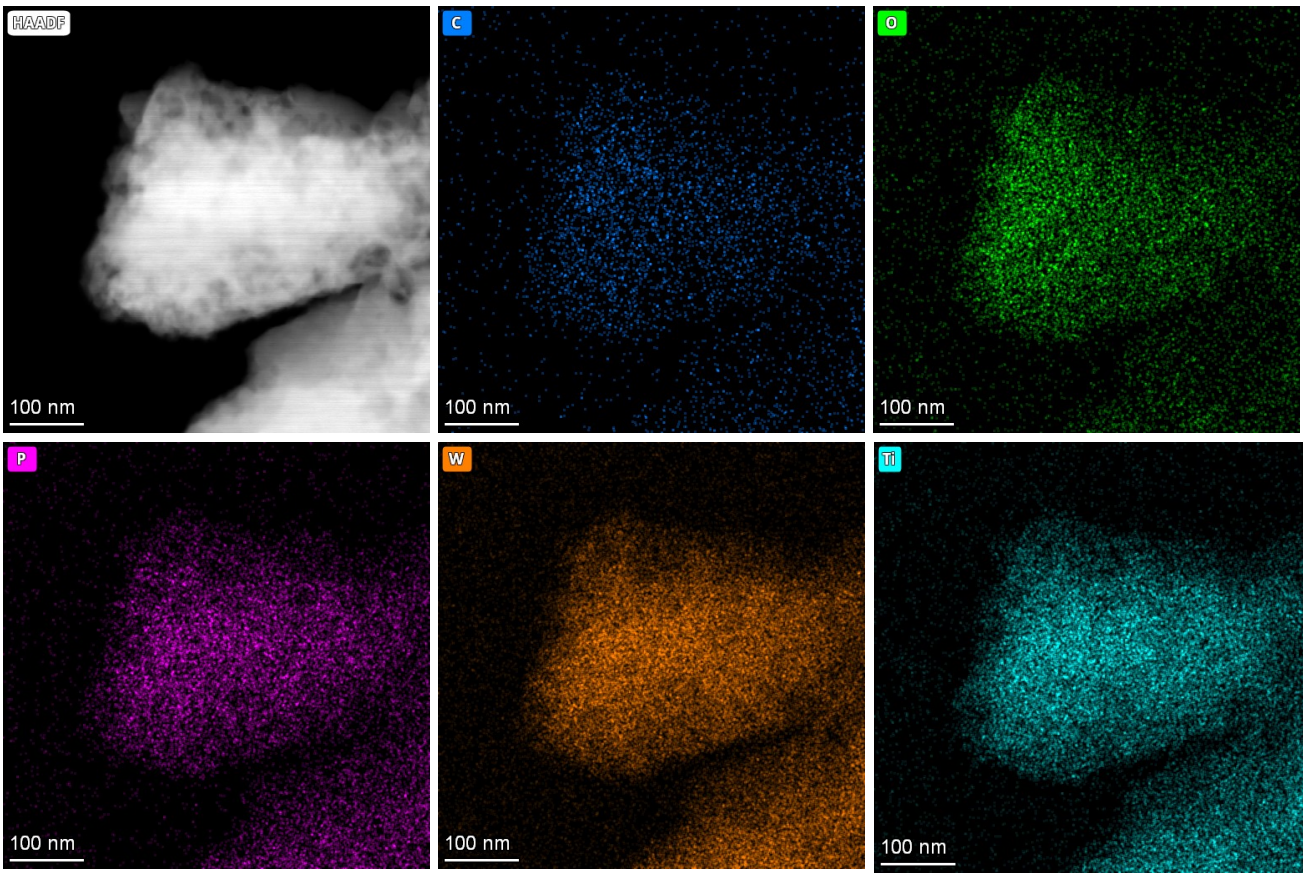

Fig. S6 STEM image and corresponding EDS elemental mapping images of Ti_{12}PTA.

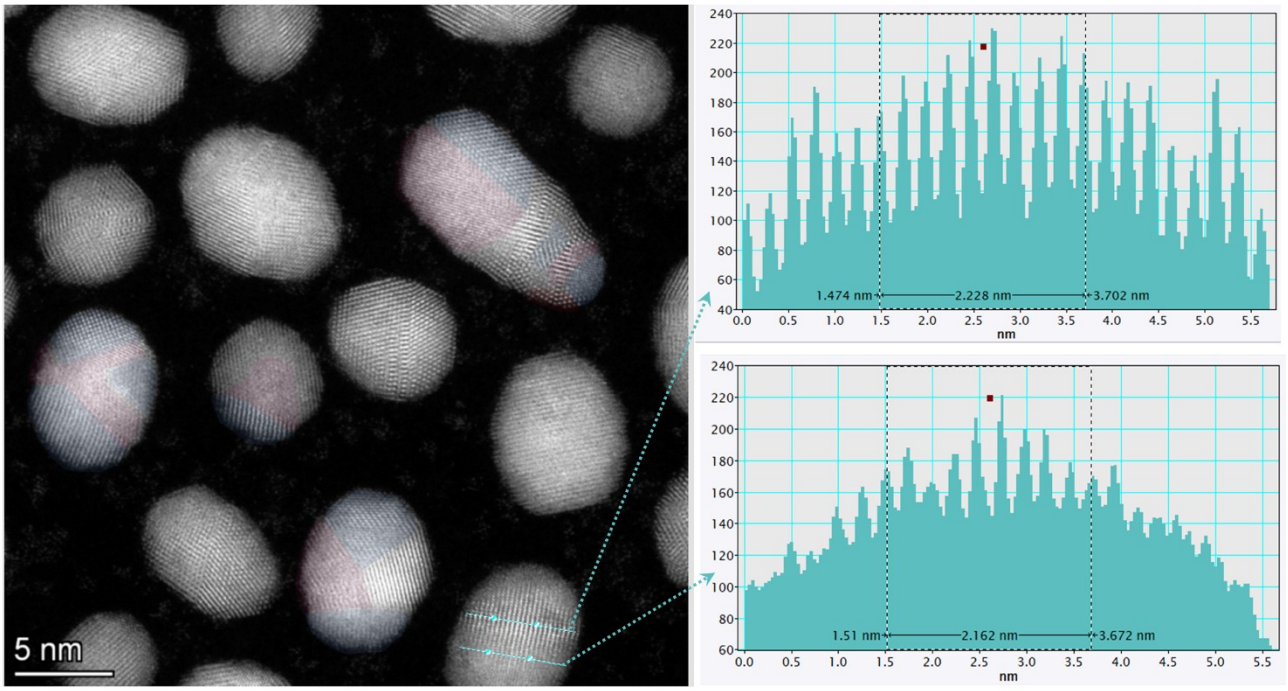

Fig. S7 High-resolution HAADF-STEM and corresponding live profile for lattice spacing at different positions of one nanoparticle on the same crystal axis.

As can be seen in the Fig. S7 that the lattice space is different at different positions of one nanoparticle on the same crystal axis, which intuitively presents the molecular heterojunction in the cocrystal system.

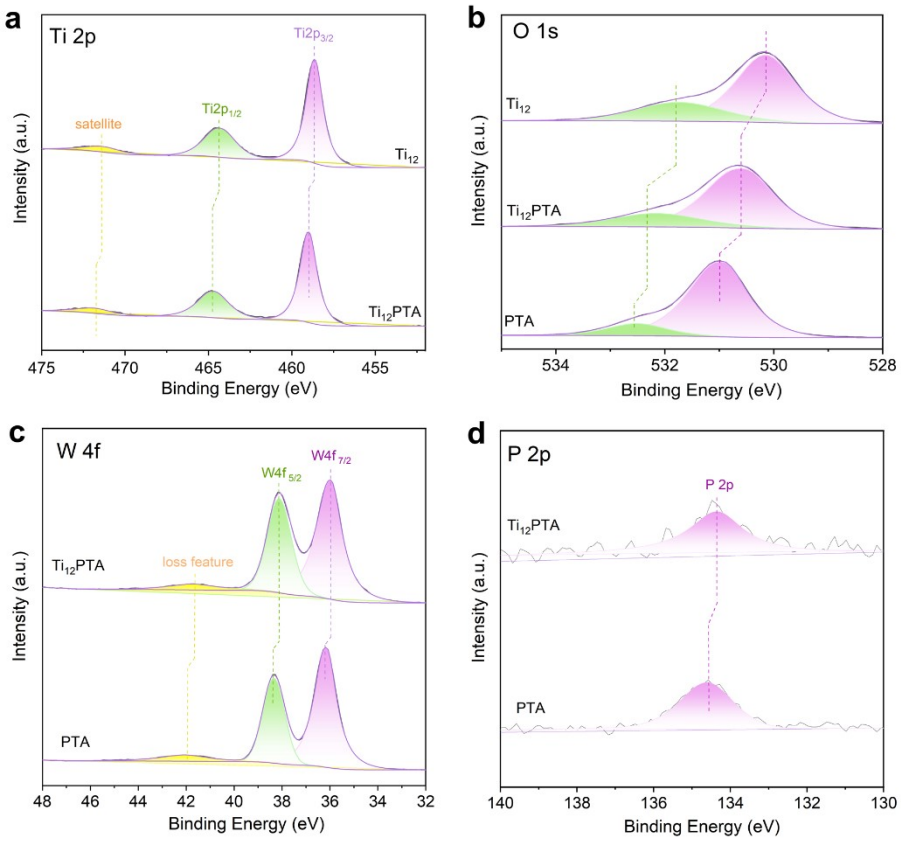

Fig. S8 High-resolution XPS spectra of (a) Ti2p in pure Ti_{12}-oxo cluster and cocrystal Ti_{12}PTA, (b) O1s in Ti_{12} cluster, PTA and cocrystal Ti_{12}PTA, (c) W4f in PTA and cocrystal Ti_{12}PTA, (d) P2p in PTA and cocrystal Ti_{12}PTA.

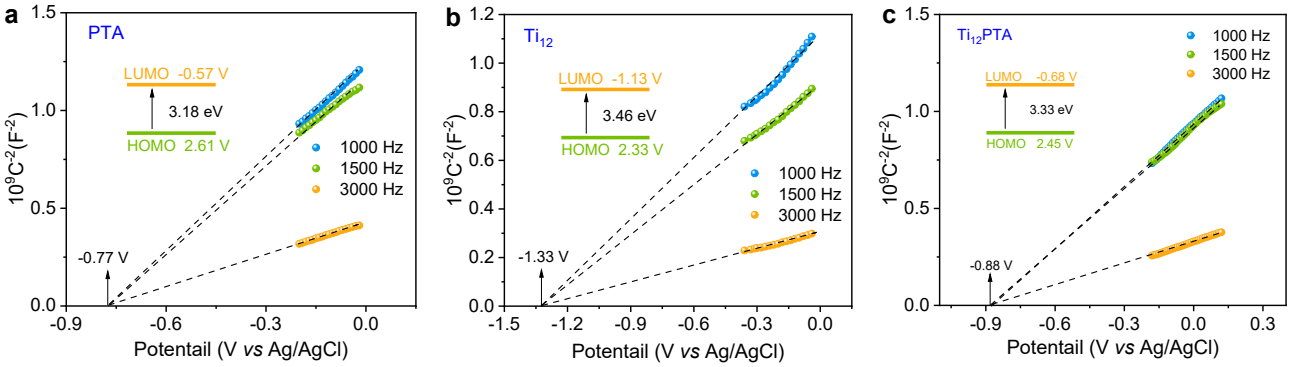

Fig. S9 Mott-Schottky plots of (a) PTA Ti_{12}, (b) Ti_{12} and (c) Ti_{12}PTA electrodes measured in Na_2SO_4 solution (0.5 M, pH ca. 7.0) at 1000 Hz, 1500 Hz and 3000 Hz.

As shown in Fig. S9, the positive slope of the obtained C^{-2} values (vs. the applied potentials) for the three clusters is consistent with that of the typical n-type semiconductors. As the intersection point is independent on the frequency, the Mott–Schottky measurements were conducted at three different frequencies (1000, 1500 and 3000 Hz) to reduce the errors. The flat band positions (V_{fb}) for PTA, Ti_{12} and Ti_{12}PTA are determined from the intersection point to be approximately -0.77 V, -1.33 V and -0.88 V vs. Ag/AgCl, respectively, which can be calculated form the Nernst equation to be -0.57 V, -1.13 V and -0.68 V vs. NHE, respectively, according to. Since it is generally accepted that the bottom of the conduction band in n-type semiconductors is very close to the flat-band potential,[S5,S6] the LUMO of PTA, Ti_{12} and Ti_{12}PTA is estimated to be -0.57 V, -1.13 V and -0.68 V vs. NHE, respectively. Combined with the bandgap energy (E_g) estimated from the Tauc plot (Fig. 2a), their HOMO levels are then calculated to be 2.33 V and 2.61 V vs. NHE, respectively. Their order and relative position agree well with the results obtained from the XPS valence band spectra (Fig. 2b), confirming the reliability of the determined energy levels.

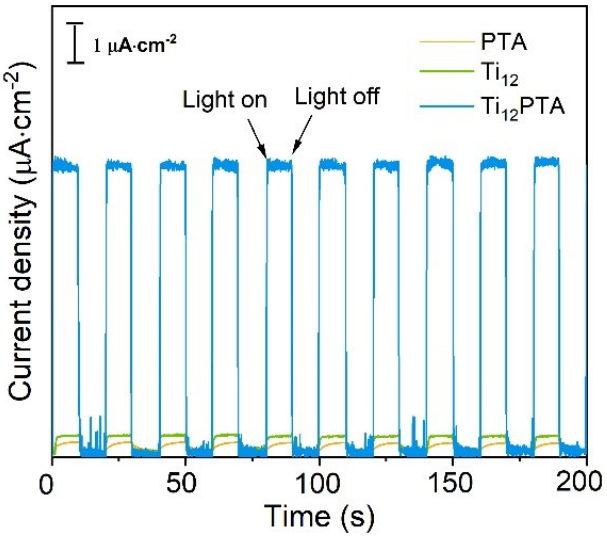

Fig. S10 Photocurrents of Ti_{12}, PTA and Ti_{12}PTA in 0.5 M Na_2SO_4 solution with triethanolamine as an electron donor under full spectrum irradiation.

To further investigate the charge transfer dynamics, we performed the photocurrent measurement on an outer-sphere system by adding triethanolamine to the electrolyte as an electron donor. Other test conditions are the same as for the inner-sphere reaction (Fig. 2d). As shown in the Fig. S10, the photocurrent of Ti_{12}PTA was 17.95 times enhanced from 0.44 μA•cm^{-1} to 7.91 μA•cm^{-1} compared to that in pure Na_2SO_4 solution after the addition of electron donor. While the individual Ti_{12} and PTA only enhanced by 1.82 and 2.1 times, respectively. The photocurrent of Ti_{12}PTA is 13.64 times and 18.83 times higher than that of Ti_{12} and PTA respectively, in the outer-sphere system, confirming its more efficient photogenerated charge separation than the individual Ti_{12} and PTA.

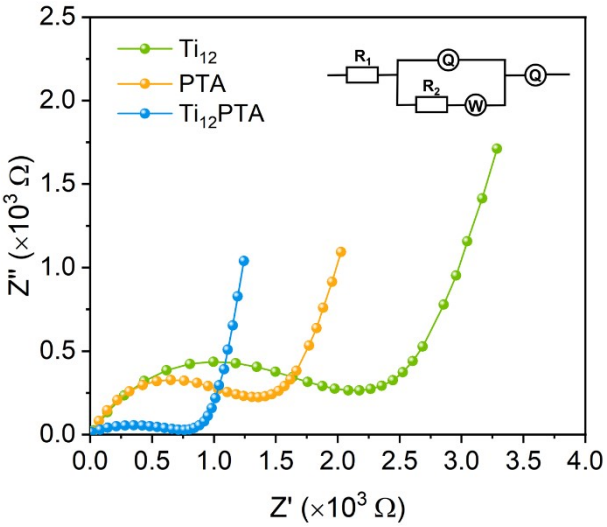

Fig. S11 Nyquist plots of Ti_{12}PTA, Ti_{12} and PTA. The inset in it is the equivalent circuit for fitting. Q and W in the equivalent circuit represent constant phase element and Warburg element, respectively.

To further confirm the superiority of Ti_{12}PTA in charge transfer and separation compared to individual PTA and Ti_{12}, we performed electrochemical impedance spectroscopy analyzes. As displayed in Fig. S11, the charge transfer resistance R_1 drops sharply from 2175.76 Ω for Ti_{12} to 1305.92 Ω for PTA and 711.64 Ω for Ti_{12}PTA, manifesting the lowest internal resistance of Ti_{12}PTA for its efficient charge transfer.

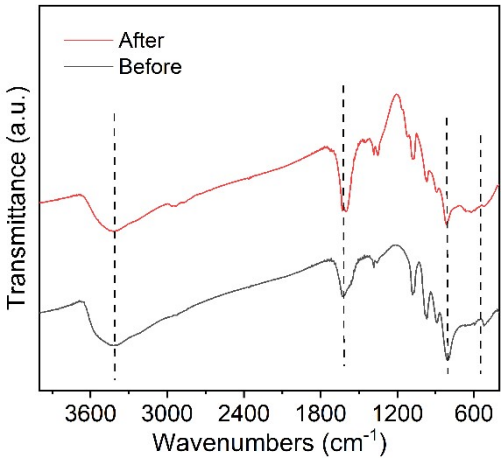

Fig. S12 FT-IR spectra of Ti_{12}PTA before and after durability test.

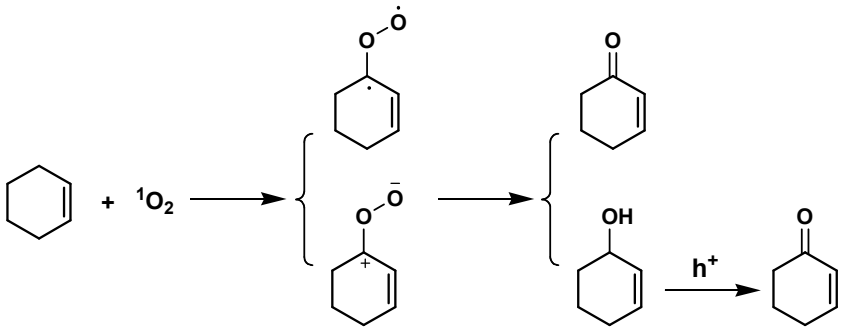

Fig. S13 Proposed mechanism for the $^1O_2$ oxidation of cyclohexene to 2-cyclohexene-1-one and 2-cyclohexene-1-ol.

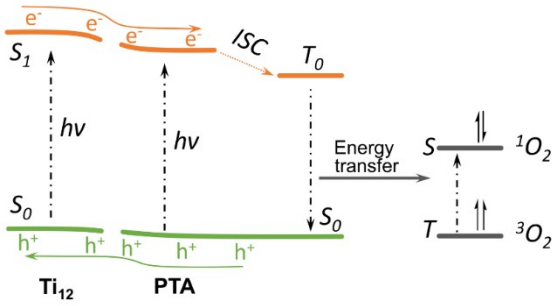

Fig. S14 Schematic illustration of the proposed mechanism for $^1O_2$ production. *S* denotes a singlet state, *T* denotes a triplet state, and ISC is abbreviation of intersystem crossing process.

Photocatalysts	Reaction solution	Light source	Total Yield（mmol•g^{-1}•h^{-1}）	Durability	Reference
$Ti_{12}PTA$	Pure cyclohexene +O_2	≥420 nm	144.0372	32 h	**This work**
$[UO_2(OPCyPh_2)_4]ClO_4 \cdot EtOH$	Acetonitrile +cyclohexene +O_2	Blue light 436 nm	73.8095	—	*Acs. Omega.* 2019, **4**, 7194−7199.
$Ti_{60}Zr_{10}Co_{30}$	Acetone +cyclohexene +O_2 (100℃)	≥420 nm	17.4238	—	*Catalysts*. 2016, **6**, 24.
$LaCoO_3$-1000℃	Acetonitrile +cyclohexene +10 bar O_2 (80℃)	≥420 nm	43.75	—	*J. Phys. Chem. C.* 2023, **127**, 5029−5038.
MNC-10	Acetone+ triphenylphosphine +cyclohexene +O_2 (75℃)	≥420 nm	7.03	18 h	*ACS. Appl. Nano. Mater.* 2022, **5**, 11723−11730.

Table S2 The performance comparison of our work with the photocatalysts for cyclohexene oxidation.

Table. S2 Bond valence sum (BVS) analysis[c] for Ti_{12}PTA.

W1 6.358	P1 5.284	Ti13 4.469
W1-O27 1.724 d=1.7195(10)	P1-O7 1.379 d=1.485(14)	Ti13-O67 1.235 d=1.713(18)
W1-O1 1.142 d=1.872(10)	P1-O80 1.354 d=1.492(15)	Ti13-O51 0.937 d=1.815(16)
W1-O78 1.096 d=1.887(8)	P1-O86 1.300 d=1.507(16)	Ti13-O99 0.853 d=1.85(2)
W1-O8 1.076 d=1.894(9)	P1-O20 1.251 d=1.521(15)	Ti13-O103 0.739 d=1.903(9)
W1-O40 1.041 d=1.906(14)		Ti13-O101 0.706 d=1.92(2)
W1-O7 0.279 d=2.393(14)		
W4 6.430	Ti1 4.251	Ti7 4.380
W4-O46 1.726 d=1.7191(10)	Ti1-O48 1.199 d=1.724(15)	Ti7-O47 1.245 d=1.710(16)
W4-O14 1.139 d=1.873(13)	Ti1-O28 0.667 d=1.941(15)	Ti7-O37 0.853 d=1.85(2)
W4-O1 1.111 d=1.882(8)	Ti1-O54 0.611 d=1.973(16)	Ti7-O21 0.812 d=1.868(19)
W4-O38 1.087 d=1.890(8)	Ti1-O64 0.600 d=1.980(14)	Ti7-O95 0.550 d=2.012(18)
W4-O6 1.084 d=1.891(9)	Ti1-O70 0.590 d=1.986(15)	Ti7-O97 0.474 d=2.067(19)
W4-O20 0.283 d=2.388(14)	Ti1-O10 0.584 d=1.990(14)	Ti7-O11 0.446 d=2.09(2)
W6 6.466	Ti4 4.410	Ti15 4.192
W6-O43 1.725 d=1.7193(10)	Ti4-O76 1.151 d=1.739(9)	Ti15-O23 0.953 d=1.809(19)
W6-O58 1.212 d=1.850(15)	Ti4-O22 0.757 d=1.894(13)	Ti15-O83 0.823 d=1.863(19)
W6-O4 1.157 d=1.867(10)	Ti4-O28 0.669 d=1.940(15)	Ti15-O93 0.765 d=1.89(2)
W6-O38 1.090 d=1.889(13)	Ti4-O54 0.642 d=1.955(15)	Ti15-O41 0.615 d=1.971(9)
W6-O66 1.008 d=1.918(16)	Ti4-O32 0.598 d=1.981(15)	Ti15-O5 0.553 d=2.01(2)
W6-O20 0.274 d=2.400(14)	Ti4-O18 0.594 d=1.984(14)	Ti15-O101 0.483 d=2.06(2)
W8 6.406	Ti6 4.396	Ti2 4.365
W8-O98 1.724 d=1.7195(10)	Ti6-O62 1.142 d=1.742(8)	Ti2-O9 1.332 d=1.685(18)
W8-O8 1.129 d=1.876(10)	Ti6-O22 0.812 d=1.868(14)	Ti2-O63 0.786 d=1.88(2)
W8-O68 1.111 d=1.882(9)	Ti6-O34 0.651 d=1.950(15)	Ti2-O95 0.745 d=1.90(2)
W8-O6 1.105 d=1.884(10)	Ti6-O64 0.656 d=1.947(15)	Ti2-O65 0.616 d=1.97(2)
W8-O36 1.050 d=1.903(14)	Ti6-O28 0.623 d=1.966(14)	Ti2-O21 0.570 d=1.999(19)
W8-O86 0.287 d=2.383(15)	Ti6-O16 0.513 d=2.038(15)	Ti2-O49 0.315 d=2.218(18)
W10 6.441	Ti8 4.205	Ti17 4.393
W10-O45 1.724 d=1.7195(10)	Ti8-O13 1.265 d=1.704(17)	Ti17-O99 0.976 d=1.80(2)
W10-O56 1.154 d=1.868(15)	Ti8-O10 0.823 d=1.863(15)	Ti17-O39 0.960 d=1.806(9)
W10-O74 1.139 d=1.873(16)	Ti8-O18 0.817 d=1.866(15)	Ti17-O63 0.950 d=1.81(2)
W10-O40 1.087 d=1.890(14)	Ti8-O26 0.660 d=1.945(15)	Ti17-O5 0.907 d=1.827(9)
W10-O102 1.087 d=1.890(9)	Ti8-O24 0.640 d=1.956(16)	Ti17-O101 0.600 d=1.98(2)
W10-O7 0.249 d=2.435(14)		

W12 6.303	Ti10 4.324	Ti19 4.215
W12-O15 1.723 d=1.7196(10)	Ti10-O35 1.452 d=1.653(16)	Ti19-O81 1.332 d=1.685(19)
W12-O78 1.102 d=1.885(8)	Ti10-O72 0.817 d=1.866(15)	Ti19-O51 0.925 d=1.82(2)
W12-O12 1.093 d=1.888(8)	Ti10-O26 0.747 d=1.899(15)	Ti19-O103 0.723 d=1.911(9)
W12-O96 1.079 d=1.893(9)	Ti10-O32 0.685 d=1.931(15)	Ti19-O11 0.725 d=1.91(2)
W12-O74 1.053 d=1.902(15)	Ti10-O18 0.623 d=1.966(15)	Ti19-O88 0.510 d=2.04(2)
W12-O7 0.253 d=2.430(15)		
W3 6.463	Ti12 4.114	Ti21 4.328
W3-O89 1.724 d=1.7195(10)	Ti12-O55 1.208 d=1.721(15)	Ti21-O11 1.279 d=1.70(2)
W3-O30 1.212 d=1.850(10)	Ti12-O24 0.825 d=1.862(15)	Ti21-O75 1.218 d=1.718(17)
W3-O44 1.099 d=1.886(8)	Ti12-O82 0.729 d=1.908(16)	Ti21-O88 0.976 d=1.80(2)
W3-O36 1.093 d=1.888(16)	Ti12-O10 0.683 d=1.932(15)	Ti21-O97 0.633 d=1.96(2)
W3-O4 1.076 d=1.894(8)	Ti12-O70 0.669 d=1.940(14)	Ti21-O25 0.222 d=2.348(9)
W3-O86 0.260 d=2.420(14)		
W7 6.430	Ti14 4.130	Ti11 4.463
W7-O61 1.723 d=1.7196(10)	Ti14-O69 0.997 d=1.792(9)	Ti11-O3 0.900 d=1.8298(10)
W7-O12 1.154 d=1.868(10)	Ti14-O16 0.971 d=1.802(9)	Ti11-O83 0.855 d=1.849(9)
W7-O104 1.108 d=1.883(11)	Ti14-O50 0.839 d=1.856(15)	Ti11-O25 0.711 d=1.917(9)
W7-O66 1.096 d=1.887(14)	Ti14-O60 0.711 d=1.917(15)	Ti11-O71 0.709 d=1.918(9)
W7-O14 1.084 d=1.891(9)	Ti14-O34 0.611 d=1.973(15)	Ti11-O93 0.669 d=1.94(2)
W7-O20 0.264 d=2.414(15)		Ti11-O85 0.618 d=1.969(9)
W2 6.496	Ti16 4.068	Ti23 4.183
W2-O73 1.723 d=1.7197(10)	Ti16-O31 1.279 d=1.700(14)	Ti23-O19 0.925 d=1.8198(10)
W2-O52 1.231 d=1.844(17)	Ti16-O32 0.784 d=1.881(15)	Ti23-O51 0.853 d=1.8498(10)
W2-O68 1.135 d=1.874(14)	Ti16-O16 0.743 d=1.901(15)	Ti23-O83 0.830 d=1.8599(10)
W2-O44 1.076 d=1.894(12)	Ti16-O72 0.652 d=1.949(15)	Ti23-O88 0.706 d=1.92(2)
W2-O56 1.058 d=1.900(14)	Ti16-O50 0.610 d=1.974(16)	Ti23-O41 0.616 d=1.9703(10)
W2-O86 0.273 d=2.402(15)		Ti23-O85 0.253 d=2.2998(10)
W9 6.240	Ti18 4.238	Ti24 4.366
W9-O17 1.724 d=1.7195(10)	Ti18-O90 1.070 d=1.766(17)	Ti24-O53 1.199 d=1.724(9)
W9-O2 1.096 d=1.887(17)	Ti18-O94 0.698 d=1.924(17)	Ti24-O92 0.669 d=1.940(16)
W9-O30 1.070 d=1.896(9)	Ti18-O42 0.665 d=1.942(16)	Ti24-O42 0.651 d=1.950(15)
W9-O84 1.067 d=1.897(13)	Ti18-O60 0.610 d=1.974(15)	Ti24-O26 0.635 d=1.959(16)
W9-O58 1.014 d=1.916(15)	Ti18-O82 0.607 d=1.976(16)	Ti24-O24 0.611 d=1.973(15)
W9-O80 0.269 d=2.407(14)	Ti18-O100 0.589 d=1.987(17)	Ti24-O94 0.602 d=1.979(18)

W5 6.372	Ti22 4.202	Ti3 4.291
W5-O33 1.724 d=1.7195(10)	Ti22-O57 1.258 d=1.706(16)	Ti3-O59 1.286 d=1.698(16)
W5-O91 1.186 d=1.858(18)	Ti22-O92 0.605 d=1.977(17)	Ti3-O65 1.030 d=1.78(2)
W5-O102 1.120 d=1.879(10)	Ti22-O42 0.590 d=1.986(15)	Ti3-O97 0.853 d=1.85(2)
W5-O84 1.093 d=1.888(9)	Ti22-O72 0.587 d=1.988(16)	Ti3-O25 0.584 d=1.990(9)
W5-O52 1.000 d=1.921(17)	Ti22-O100 0.586 d=1.989(18)	Ti3-O71 0.539 d=2.02(2)
W5-O80 0.249 d=2.435(15)	Ti22-O50 0.576 d=1.995(15)	

W11 6.194
W11-O87 1.723 d=1.7196(10)
W11-O96 1.123 d=1.878(11)
W11-O104 1.087 d=1.890(9)
W11-O91 1.025 d=1.912(16)
W11-O2 0.973 d=1.931(16)
W11-O80 0.262 d=2.416(16)

[c]Vi =ΣSij = Σexp[(r1 -rij)/B], where r0 is the length of a single bond (here r1 = 1.921 for W -O; 1.604 for P -O ; 1.791 for Ti -O), r1 is the bond length between atoms i and j; B is a constant, the “universal parameter” ~0.37 Å; Sij is the valence of a bond between atoms i and j; Vi is the sum of all bond valences of the bonds formed by a given atom.[S7]

References

S1 A. Bondi, *J. Phys. Chem.* 1964, **68**, 441–451.

S2 L. Krause, R. Herbst-Irmer and G. M. Sheldrick, *J. Appl. Crystallogr.* 2015, **48**, 3–10.

S3 R. E. Gannon, V. J. Krukonis and T. Schoenberg, *Product R&D.* 1970, **9**, 343–347.

S4 A. Spek, *J. Appl. Crystallogr.,* 2003, **36**, 7–13.

S5 Z. Z. Zhang, J.L. Long, L.F. Yang, W.K. Chen, W.X. Dai, X.Z. Fu and X.X. Wang, *Chem. Sci*. 2011, **2**, 1826–1830.

S6 K. Maeda, K. Sekizawa and O. Ishitani, *Chem. Commun*. 2013, **49**, 10127–10129.

S7 I. D. Brown, *Chem. Rev.,* 2009, **109**, 6858–919.